Supporting Information

A Multifunctional Cobalt-Oragnic Framework for Proton Conduction and Selective Sensing of Fe^{3+} Ions

Wen-Sha Zhang,[a†] Guang-Qing Wang,[a] Yu-Xin Wang,[a] Yan-Li Yang,[a] Xue Bai,[a] Hong Cui,[a] Ying Lu*[a] and Shu-Xia Liu*[a]

[a]*Key Laboratory of Polyoxometalate and Reticular Material Chemistry of the Ministry of Education, College of Chemistry, Northeast Normal University, Changchun, Jilin 130024, P. R. China.*

E-mail: luy968@nenu.edu.cn; liusx@nenu.edu.cn

Experimental Section

Proton conductivity measurement

For single-crystal measurements, The index of the crystal plane of the single crystal sample was realized by X-ray diffraction patterns . The AC impedance was tested on single crystal samples of **1** using the conventional two-contact wire paste method. Two crystals with dimensions of 1.00× 0.35× 0.10 mm^3 and 0.90× 0.40× 0.15 mm^3, respectively, were carefully bonded to a soft silver wire (0.1 mm) using conductive silver glue, and the samples were connected to a homemade electrode holder for the AC impedance test. The single crystals was measured at frequencies ranging from 10^7 to 0.1 Hz as the temperatures were varied from 25 to 55 °C and/or as the relative humidities (RH) were varied from 55 to 95%. The conductivity of the samples was deduced from the Debye semicircle in the Nyquist plot. The proton conductivities were calculated using the equation: $\sigma = L / (S \cdot R)$, where L and S are the thickness (cm) and cross-sectional area (cm^2) of the tablet, respectively. The σ is the proton conductivity (S cm^{-1}). The activation energy was calculated from the following Arrhenius equation:

$$\sigma T=\sigma_0 \exp(-Ea/k_B T)$$

Where σ is the proton conductivity, k_B is the Boltzmann constant, σ_0 is the prexponential factor, and T is the temperature.

Figures

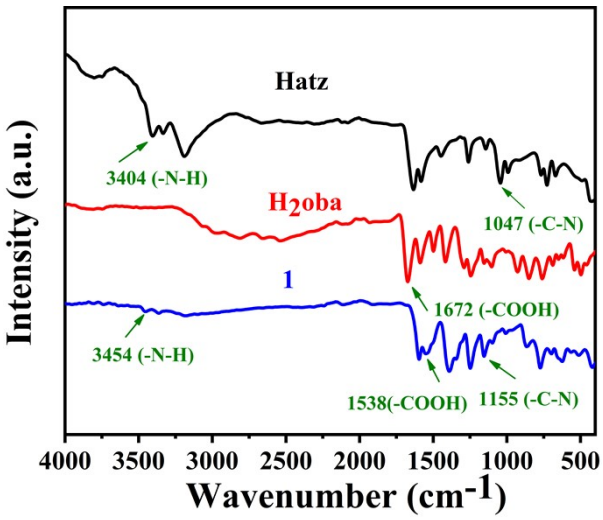

Fig. S1. IR spectrum of compound **1** 、H_2oba and Hatz.

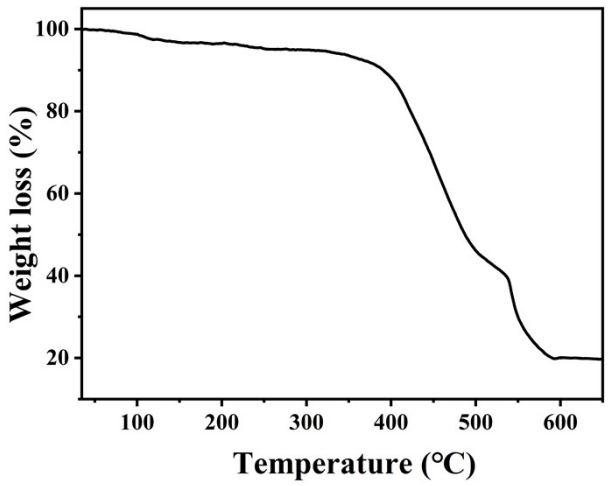

Figure S2. The TG plot of compound **1**.

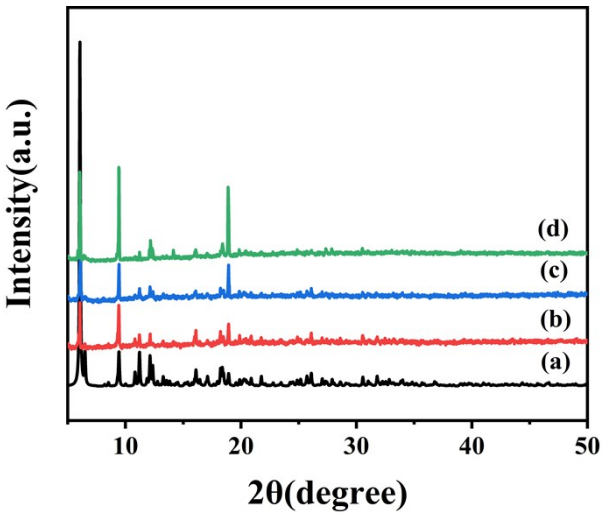

Figure S3. Powder XRD patterns of (a) simulated from the single-crystal data of **1**, (b) as-synthesized product, (c) **1** immersed in water for **1** week and (d) **1** immersed in $Fe(NO_3)_3$ aqueous solution for 24 h.

Figure S4. The photographs of the single crystal of **1** under 65% (left) and 95% RH(right).

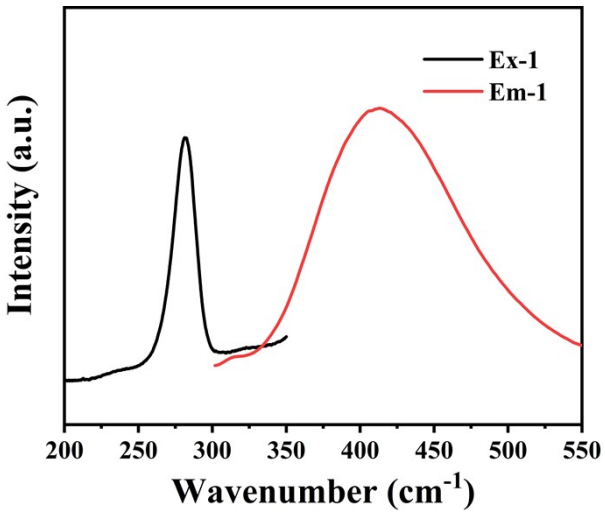

Figure S5. The luminescent spectra of **1** in water. (Ex:5nm; Em:10nm)

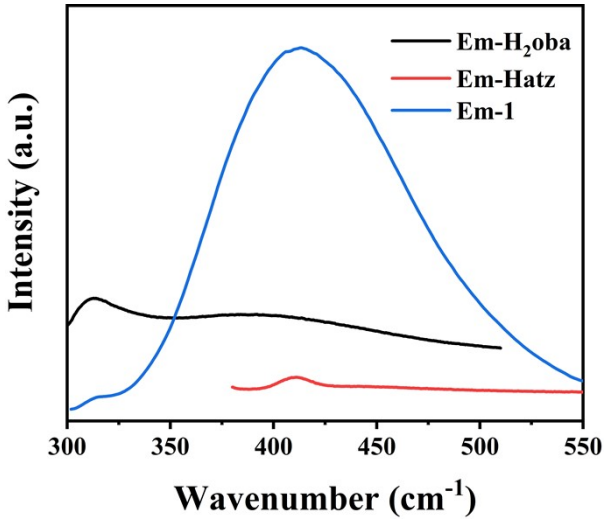

Figure S6. The luminescent spectra of **1**、H_2oba and Hatz in water.

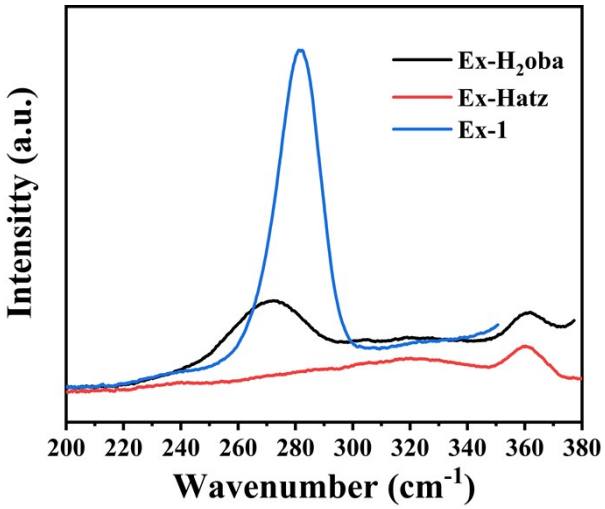

Figure S7. The luminescent spectra of **1**、H_2oba and Hatz in water.

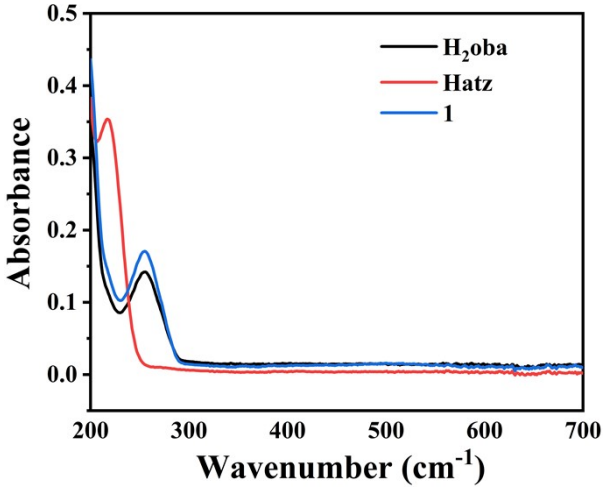

Figure S8. Liquid UV-Vis spectra of **1**、H_2oba and Hatz in water.

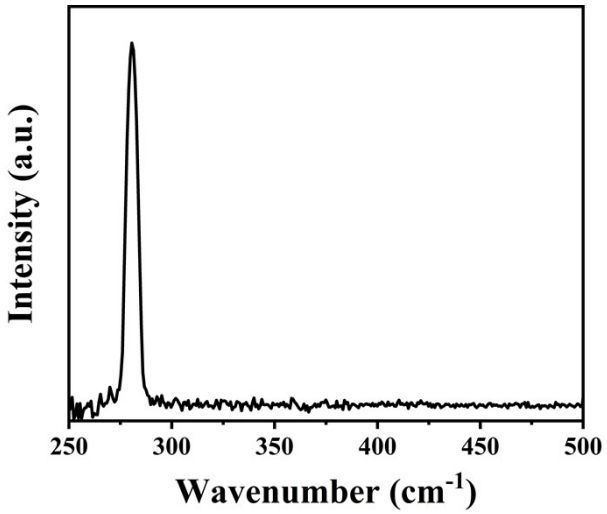

Figure S9. The fluorescent quantum yield of **1.**

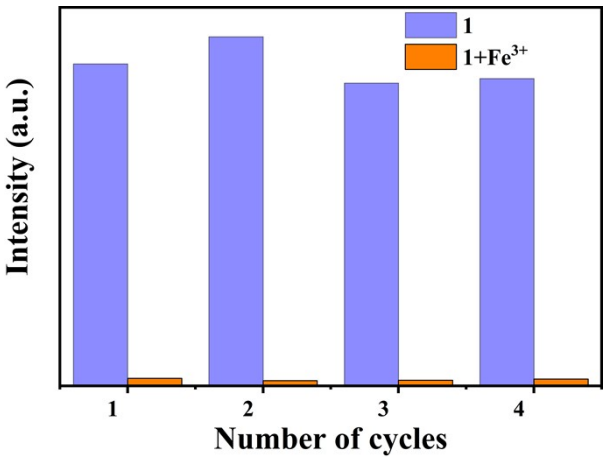

Figure S10. The fluorescence intensity of **1** after four times of recycling.

Tables

Table S1. Compare the proton conductivity of **1** with that of other conductors

	Conductivity		Conditions	References
	in-direction	out-of-direction		
1	**1.1×10^{-3}**	**9.1×10^{-6}**	**55℃，95% RH**	**This work**
$[Eu_2(CO_3)(ox)_2(H_2O)_2]\cdot 4H_2O$	2.1×10^{-3}	4.9×10^{-7}	150℃	1
$[Co^{III}Ca^{II}(notpH_2)\cdot(H_2O)_2]ClO_4\cdot 4$	1.0×10^{-3}	4.4×10^{-8}	25℃，95% RH	2
$[Cu_2(Htzehp)_2(4,4'\text{-bipy})]\cdot 3H_2O$	1.4×10^{-3}	2.5×10^{-5}	80℃，95% RH	3
$[H_3O][(VO_2)_3(SeO_3)_2]$	5.9×10^{-5}	7.3×10^{-8}	90℃，95% RH	4
$[Ba(H_3L)(H_2O)]\cdot H_2O$	1.1×10^{-4}	1.2×10^{-5}	22℃，95% RH	5
$(DAS)(TMA)_2\cdot 2H_2O$	2.4×10^{-1}	2.4×10^{-3}	80℃，60% RH	6
$[P_2Mo_5O_{23}][C_7H_7N_2]_6\cdot H_2O$	1.9×10^{-2}	8.9×10^{-5}	50℃，98% RH	7
Co-MOF-74	4.5×10^{-3}	8.0×10^{-6}	90 ℃，95% RH	8
$[Zn(H_2PO_4)_2(TzH)_2]$	1.1×10^{-4}	2.9×10^{-6}	130℃	9
Im-Suc	4.9×10^{-7}	3.6×10^{-9}	115℃	10

Table S2. Comparison of various MOFs for the detection of Fe^{3+} ions

Compounds	Detection limit (μM)	K_{sv} (M^{-1})	Reference
$Co_6(oba)_4(Hatz)(atz)(H_2O)_2(\mu_3\text{-}OH)_2(\mu_2\text{-}OH)\cdot H_2O$	**2.98**	**9.55×10^4**	**This work**
$\{[Eu_2(ppda)_2(npdc)(H_2O)]\cdot H_2O\}_n$	16.60	1.64×10^5	11
$[Zn(TIBTC)(DMA)]\cdot[NH_2(CH_3)_2]$	3.45	9.71×10^4	12
$[Cd(TIBTC)(H_2O)]\cdot[NH_2(CH_3)_2]\cdot DMA$	5.51	2.43×10^4	12
FJI-C8·(Zn)	23.30	8.24×10^3	13
Cd-CP	3.24	4.10×10^4	14
Tb-MOF-A	12.70	4.04×10^4	15
[Zn(L)(bpp)]DMF	7.60	2.56×10^4	16

Table S3. Selected bond lengths [Å] and angles [°] for **1**

Co1-N2	2.085(3)	Co5-O17[1]	2.068(3)
Co2-N3[1]	2.114(3)	Co6-O24[2]	2.086(3)
Co2-O10[2]	2.063(3)	Co6-O15	2.082(2)
Co3-O5	2.041(3)	Co7-O15	2.047(2)
Co3-N6	2.121(3)	Co7-O14	2.166(3)
O25-Co1-O6[1]	89.98(12)	O25-Co1-O28	94.92(12)
O10[2]-Co2-O6	90.57(11)	O7-Co2-O6	120.76(12)
O16-Co3-O26	58.14(10)	O5-Co3-O6	114.84(12)
O8-Co4-O15	169.97(11)	O8-Co4-O16[1]	106.79(11)
O16-Co5-O16[1]	177.04(14)	O17[1]-Co5-O16	88.20(10)
O15-Co6-O24[2]	94.34(10)	O15[4]-Co6-O24[5]	94.34(10)
O15-Co7-N5	177.57(11)	O15-Co7-O23[2]	90.47(10)

[1]1-X, +Y, 3/2-Z; [2]1/2-X, 1/2+Y, +Z; [3]-1/2+X, -1/2+Y, 3/2-Z; [4]-X,+Y, 3/2-Z; [5]-1/2+X, 1/2+Y, 3/2-Z

Table S4. The observed IR bands for **1**.

Bands	Wavenumber (cm^{-1})	Bands	Wavenumber (cm^{-1})
$\upsilon_{str}(H_2O)$	3000-3600(s)	$\upsilon_{sy.\ str}$(carboxylate)	1392
υ_{str}(N-H)	3457, 3358(s)	υ_{str}(C-N)	1247, 1149,1094
υ_{str}(aromatic C-H)	3086(w)	δ(aromatic C-H)$_{in\ plane\ bending}$	1040(m), 1012(s)
$\upsilon_{asy.\ str}$(carboxylate)	1615(s)	δ(aromatic C-H)$_{out\ of\ plane\ bending}$	886(s), 868(m), 775(m),764(m),
υ_{str}(aromatic C=C)	1548(m), 1596(m)	δ(carboxylate)$_{bending}$	712(s), 690(m), 656(m)

Table S5. The O···O and O···N bonds lengths (Å) for **1** (H not directly observed).

Atoms involved	Length (Å)	Atoms involved	Length (Å)
O4-N1	3.73	O21-N1	3.11
O15-O21	2.95	O15-O16	2.90
O14-N4	3.24	O6-O10	2.95
O10-N4	3.95	O7-N4	3.02
O15-O17	3.02	O16-O17	3.01
O15-O12	2.96	O12-O7	3.18
N10-O12	3.18	O14-O16	2.97

References

1. Q. Tang, Y. Liu, S. Liu, D. He, J. Miao, X. Wang, G. Yang, Z. Shi and Z. Zheng, High Proton Conduction at above 100 °C Mediated by Hydrogen Bonding in a Lanthanide Metal–Organic Framework, *J. Am. Chem. Soc.*, 2014, **136**, 12444-12449.
2. S.-S. Bao, N.-Z. Li, J. M. Taylor, Y. Shen, H. Kitagawa and L.-M. Zheng, Co–Ca Phosphonate Showing Humidity-Sensitive Single Crystal to Single Crystal Structural Transformation and Tunable Proton Conduction Properties, *Chem. Mater.*, 2015, **27**, 8116-8125.
3. R. Li, S.-H. Wang, X.-X. Chen, J. Lu, Z.-H. Fu, Y. Li, G. Xu, F.-K. Zheng and G.-C. Guo, Highly Anisotropic and Water Molecule-Dependent Proton Conductivity in a 2D Homochiral Copper(II) Metal–Organic Framework, *Chem. Mater.*, 2017, **29**, 2321-2331.
4. G. Xu, K. Otsubo, T. Yamada, S. Sakaida and H. Kitagawa, Superprotonic Conductivity in a Highly Oriented Crystalline Metal–Organic Framework Nanofilm, *J. Am. Chem. Soc.*, 2013, **135**, 7438-7441.
5. A. Javed, T. Wagner, S. Wöhlbrandt, N. Stock and M. Tiemann, Proton Conduction in a Single Crystal of a Phosphonato-Sulfonate-Based Coordination Polymer: Mechanistic Insight, *Chemphyschem.*, 2020, **21**, 605-609.
6. Y. Wang, M. Zhang, Q. Yang, J. Yin, D. Liu, Y. Shang, Z. Kang, R. Wang, D. Sun and J. Jiang, Single-crystal-to-single-crystal transformation and proton conductivity of three hydrogen-bonded organic frameworks, *Chem. Commun.*, 2020, **56**, 15529-15532.
7. X.-L. Cao, S.-L. Xie, S.-L. Li, L.-Z. Dong, J. Liu, X.-X. Liu, W.-B. Wang, Z.-M. Su, W. Guan and Y.-Q. Lan, A Well-Established POM-based Single-Crystal Proton-Conducting Model Incorporating Multiple Weak Interactions, *Chem. – Eur. J.,* 2018, **24**, 2365-2369.
8. S. Hwang, E. J. Lee, D. Song and N. C. Jeong, High Proton Mobility with High Directionality in Isolated Channels of MOF-74, *Acs. Appl. Mater. Inter.*, 2018, **10**, 35354-35360.
9. D. Umeyama, S. Horike, M. Inukai, T. Itakura and S. Kitagawa, Inherent Proton Conduction in a 2D Coordination Framework, *J. Am. Chem. Soc.*, 2012, **134**, 12780-12785.
10. Y. Sunairi, A. Ueda, J. Yoshida, K. Suzuki and H. Mori, Anisotropic Proton Conductivity Arising from Hydrogen-Bond Patterns in Anhydrous Organic Single Crystals, Imidazolium Carboxylates, *J. Phys.Chem. C.*, 2018, **122**, 11623-11632.

11. Z. Zhan, X. Liang, X. Zhang, Y. Jia and M. Hu, A water-stable europium-MOF as a multifunctional luminescent sensor for some trivalent metal ions (Fe^{3+}, Cr^{3+}, Al^{3+}), PO_4^{3-} ions, and nitroaromatic explosives, *Dalton Trans.*, 2019, **48**, 1786-1794.
12. C.-H. Liu, Q.-L. Guan, X.-D. Yang, F.-Y. Bai, L.-X. Sun and Y.-H. Xing, Polyiodine-Modified 1,3,5-Benzenetricarboxylic Acid Framework Zn(II)/Cd(II) Complexes as Highly Selective Fluorescence Sensors for Thiamine Hydrochloride, NACs, and Fe^{3+}/Zn^{2+}, *Inorg. Chem.*, 2020, **59**, 8081-8098.
13. L. C. Gómez-Aguirre, B. Pato-Doldán, A. Stroppa, L.-M. Yang, T. Frauenheim, J. Mira, S. Yáñez-Vilar, R. Artiaga, S. Castro-García, M. Sánchez-Andújar and M. A. Señarís-Rodríguez, Coexistence of Three Ferroic Orders in the Multiferroic Compound $[(CH_3)_4N][Mn(N_3)_3]$ with Perovskite-Like Structure, *Chem.–Eur. J.*, 2016, **22**, 7863-7870.
14. Y. e. Yu, Y. Wang, H. Yan, J. Lu, H. Liu, Y. Li, S. Wang, D. Li, J. Dou, L. Yang and Z. Zhou, Multiresponsive Luminescent Sensitivities of a 3D Cd-CP with Visual Turn-on and Ratiometric Sensing toward Al^{3+} and Cr^{3+} as Well as Turn-off Sensing toward Fe^{3+}, *Inorg. Chem.*, 2020, **59**, 3828-3837.
15. H.-H. Yu, J.-Q. Chi, Z.-M. Su, X. Li, J. Sun, C. Zhou, X.-L. Hu and Q. Liu, A water-stable terbium metal–organic framework with functionalized ligands for the detection of Fe^{3+} and $Cr_2O_7^{2-}$ ions in water and picric acid in seawater, *Crystengcomm.*, 2020, **22**, 3638-3643.
16. Z. Chen, X. Mi, S. Wang, J. Lu, Y. Li, D. Li and J. Dou, Two novel penetrating coordination polymers based on flexible S-containing dicarboxylate acid with sensing properties towards Fe^{3+} and $Cr_2O_7^{2-}$ ions, *J. Solid. State. Chem.*, 2018, **261**, 75-85.